Electronic Supplementary Material (ESI) for Journal of Materials Chemistry A.

Supporting Information

Environment stable ionic organohydrogels as Self-Powered Integrated System for wearable electronics

Jianren Huang, Jianfeng Gu, Jiantao Liu, Jinquan Guo, Huiyong Liu, Kun Hou, Xiancai Jiang, Xiaoxiang Yang, Lunhui Guan* *

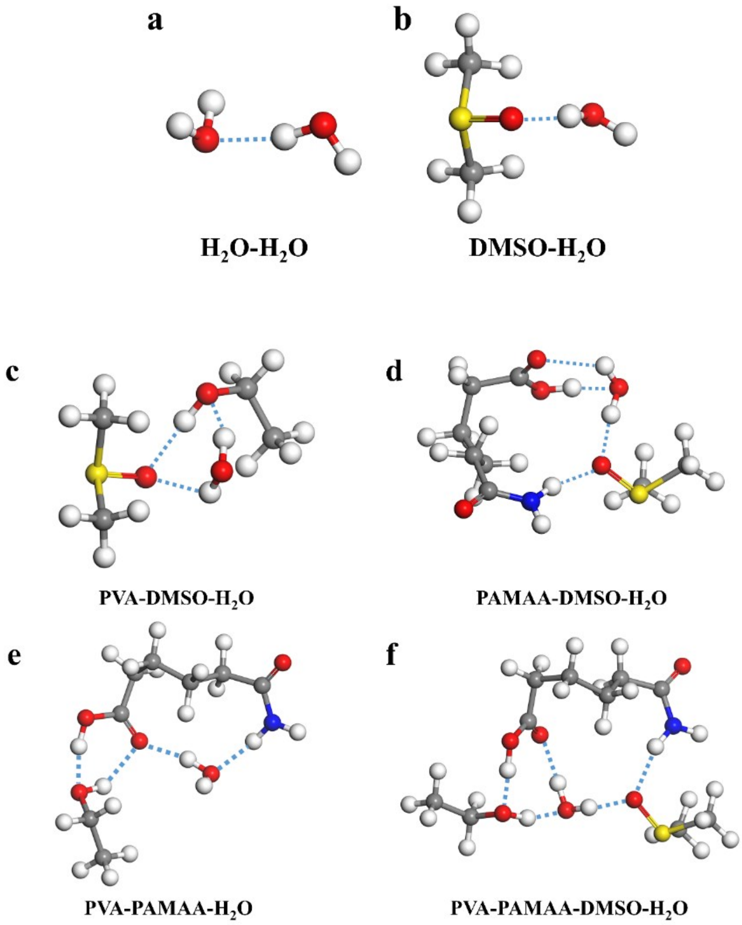

Figure S1. DFT analysis and hydrogen bonding interactions of (a)H_2O-H_2O, (b) DMSO-H_2O, (c) PVA-DMSO-H_2O, (d) PAMAA-DMSO-H_2O, (e) PVA-PAMAA-H_2O, (f) PVA-PAMAA-DMSO-H_2O.

Computational details

To further understand their intermolecular interactions, density functional theory (DFT) calculations were carried out using Dmol^3 module in Materials Studio software package. [1] The geometry optimizations were performed using the Perdew-Burke-Ernzerh of (PBE)[2] modification of the generalized gradient approximation (GGA)[3] with the Grimme[4,5] custom method for DFT-D correction together with the doubled numerical basis set plus polarization basis sets (DNP, including polarization *d*-function), and the cutoff energy for the plane-wave basis set is set to be 240.0 eV while the *k*-point is set to 7×7×1 to achieve high accuracy. The core electrons were treated by the DFT semi-core pseudo potentials, and a global orbital cutoff of 3.2 Å and a Fermi smearing of 0.005 Ha were used for the simulations. The convergence criteria including self-consistent field (SCF) tolerance of 1.0×10^{-5} Ha per atom, a maximum force tolerance of 0.002 Ha Å^{-1}, an energy tolerance of 1.0×10^{-5} Ha per atom and a maximum displacement tolerance of 0.005 Å were employed. The interaction energy (ΔE_{int}) is the difference between the total energy of the complex and the sum of total energies of its components.

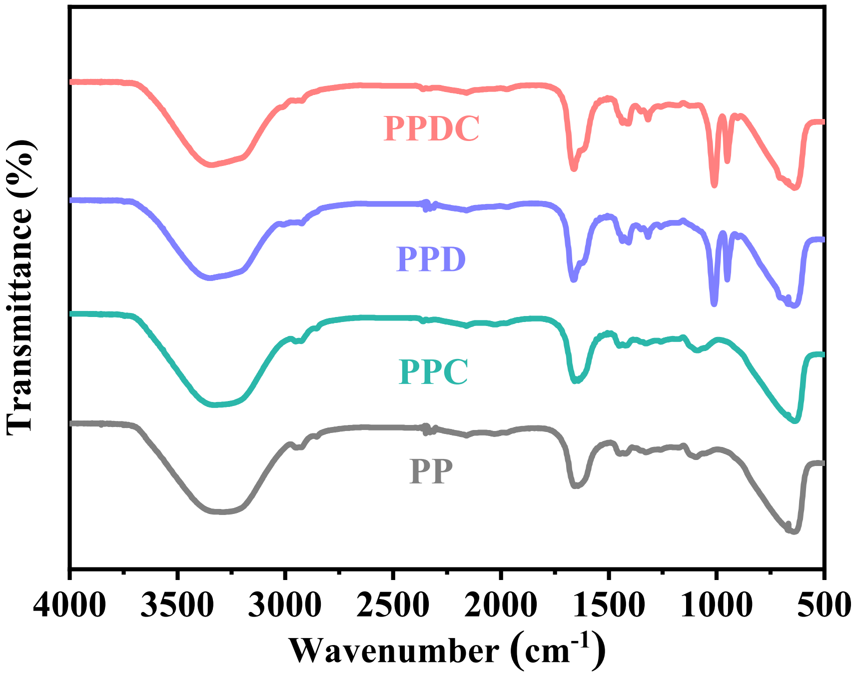

Figure S2. FT-IR spectra of PP, PPC, PPD and PPDC hydrogel in the wavenumber range of 4000-500 cm^{-1}.

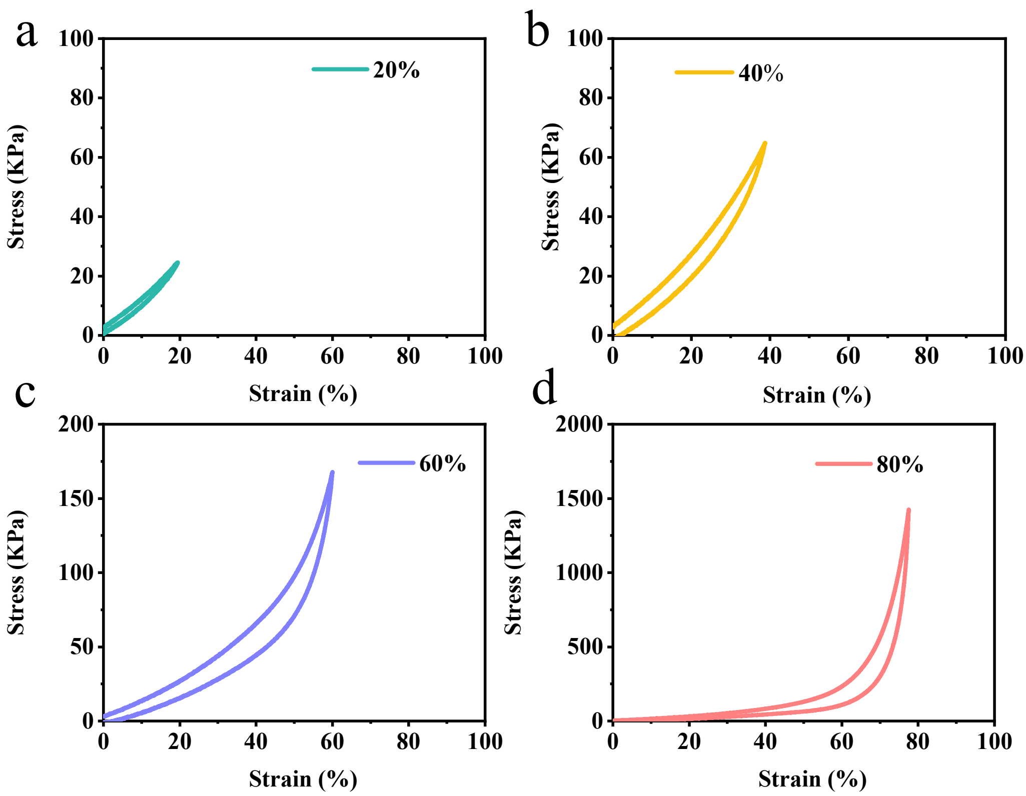

Figure S3. Compression-recovery measurements of the PPDC hydrogel at different strain, (a) 20%, (b) 40%, (c) 60% and (d) 80%.

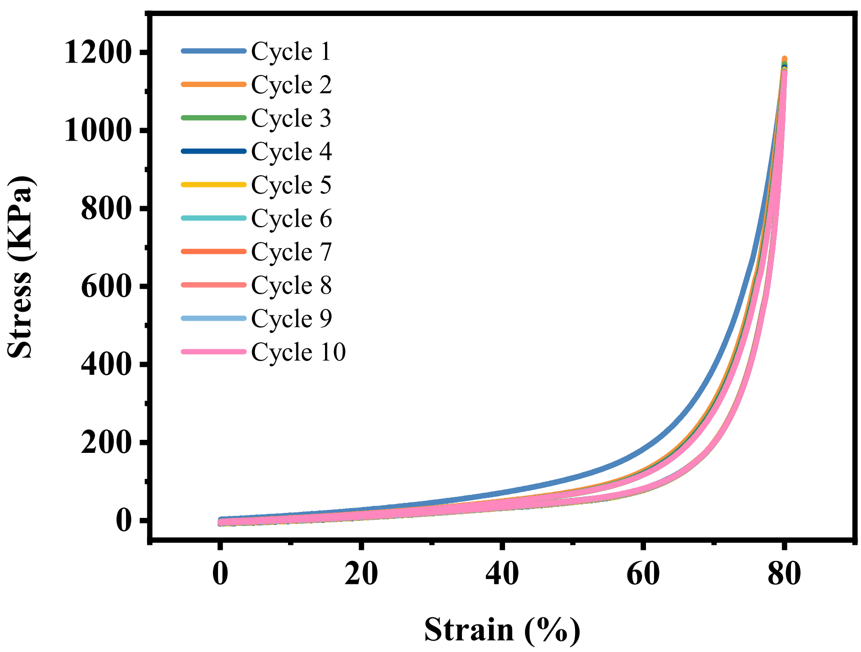

Figure S4. Ten successive cyclic loading-unloading curves of the PPDC hydrogel without a resting interval between two consecutive tests.

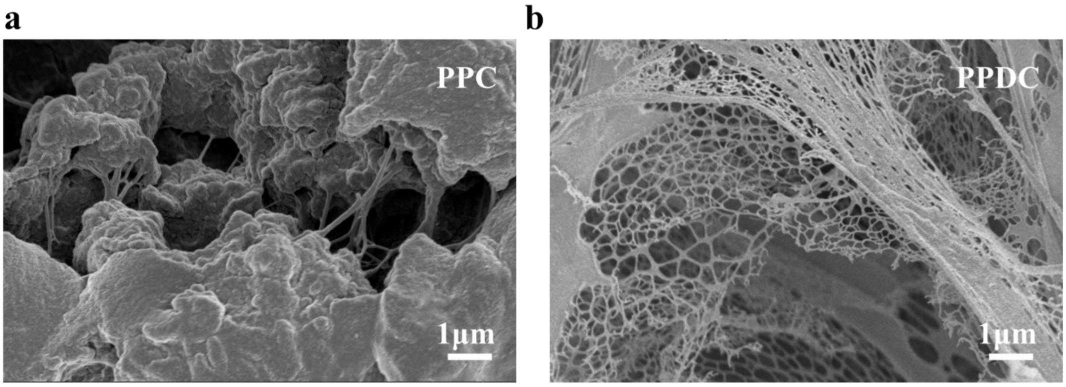

Figure S5. SEM images of (a) PPC hydrogel and (b) PPDC hydrogel.

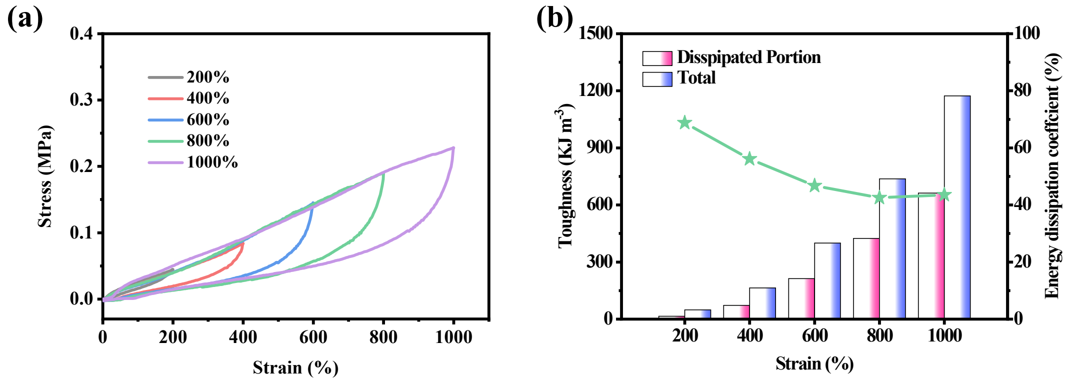

Figure S6. Mechanical properties of PPDC hydrogel (a) Loading-unloading curves and (b) corresponding toughness/energy dissipation at different maximum strain.

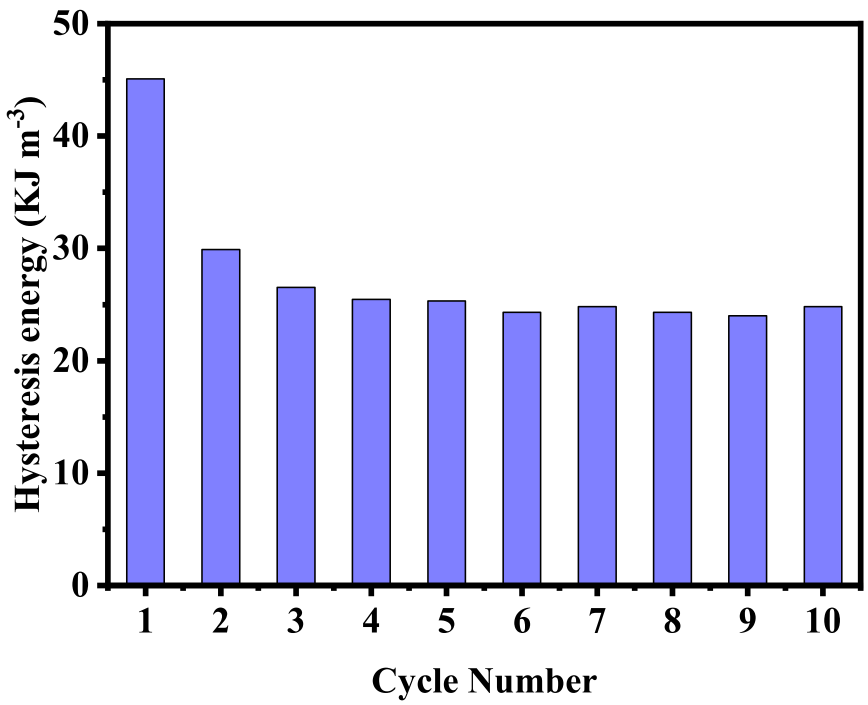

Figure S7. The dissipated energies of ten successive loading-unloading cycles at tensile strain of 300%.

The PPDC hydrogel also had outstanding mechanical durability behaviors Besides, the hysteresis loop curve with a residual strain became inconspicuous in subsequent cycles the dissipated energy kept almost constant of 25 kJ m^{-3} after the first cyclic.

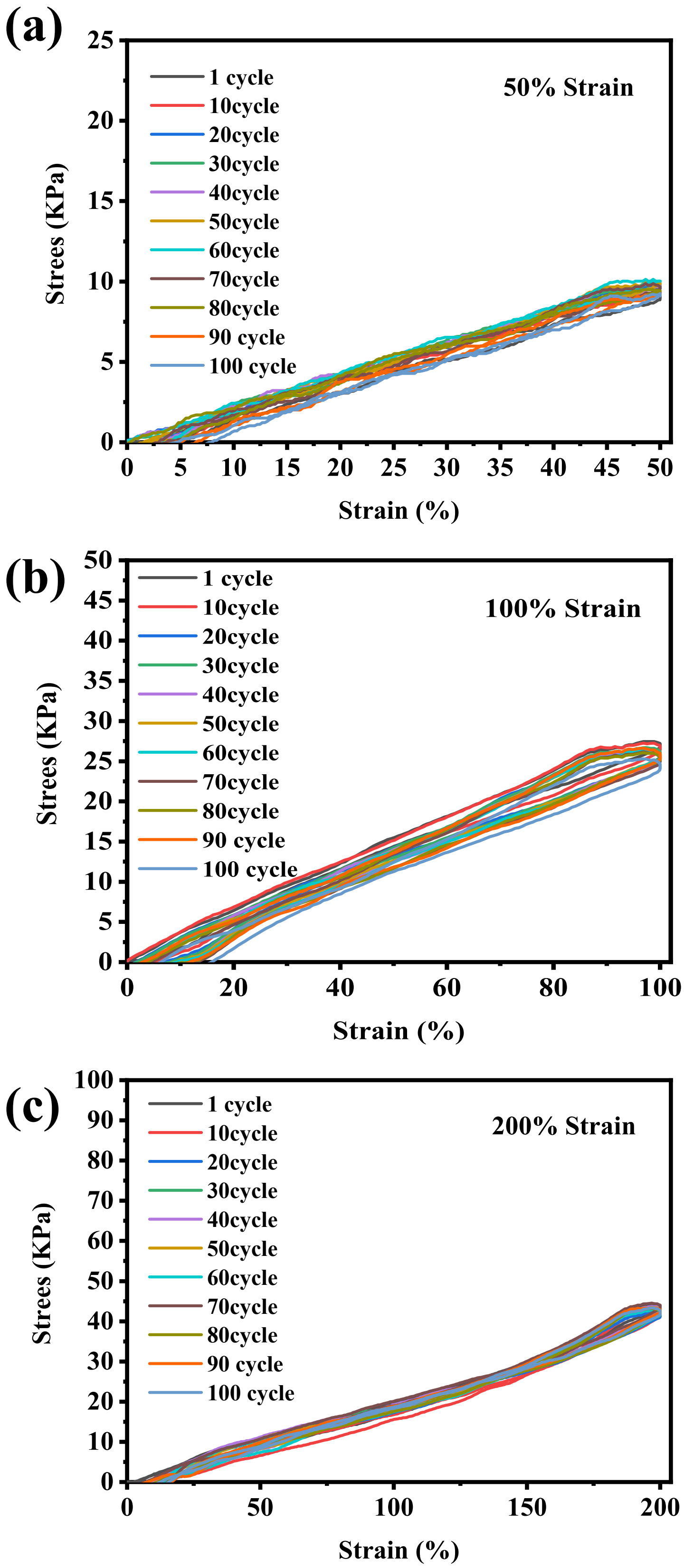

Figure S8. One hundred consecutive cycles of loading and unloading for PPDC hydrogel at (a)50% (b)100% (c)200% tensile strain with with 1min resting time between two consecutive tests.

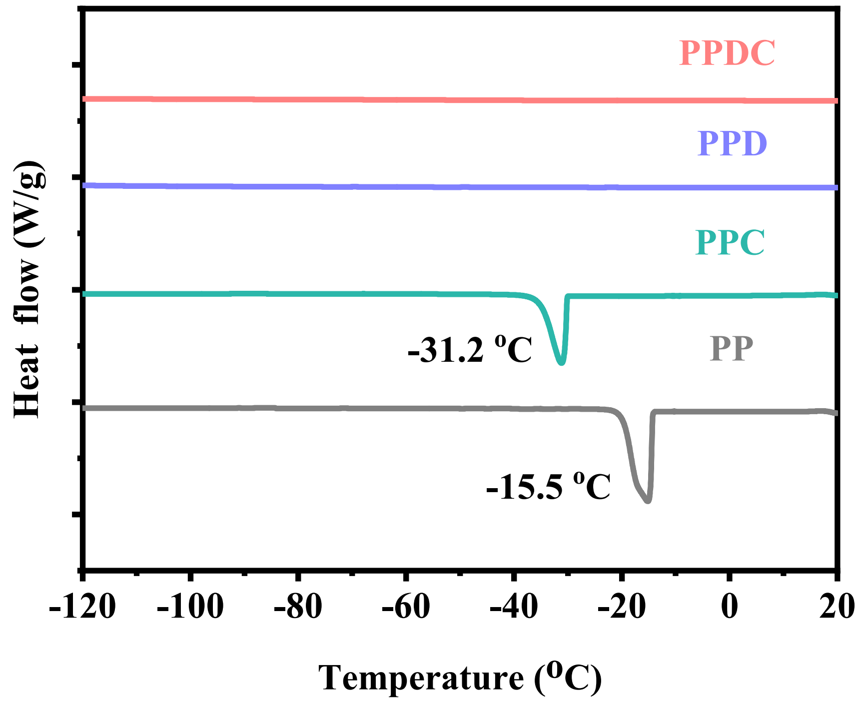

Figure S9. The DSC curves of the PP, PPC, PPD and PPDC hydrogel ranging from -120 °C to 20 °C.

An endothermic peak at 15.5°C was observed in the absence of $CaCl_2$ and DMSO (PP hydrogels), corresponding to the freezing of free water entrapped within the PVA/PAMAA crosslink network. The introduction of $CaCl_2$ leads the respective peaks to shift to lower temperatures and to become smaller, indicating the $CaCl_2$ enhances interactions of water around the polymer network. The Calcium chloride $CaCl_2$ significantly alters the state of water within the hydrogels, preventing freezing or resisting ice formation. Additionally, the DSC data of DMSO introduced PVA/PAMAA based hydrogels presents no exothermic peak, indicating that the PPDC and PPD hydrogels have a freezing point below -120 °C, completely inhibits water in the hydrogel from freezing.[6]

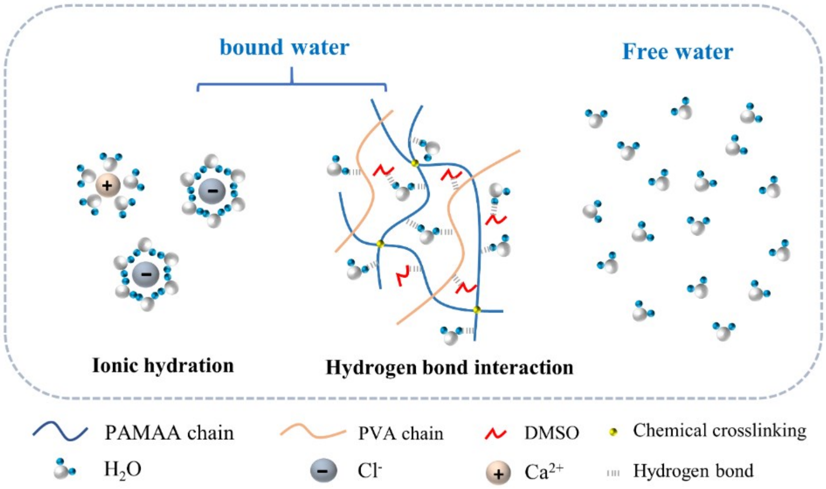

Figure S10. Schematic of the hydration of $CaCl_2$ in water and the hydrogen bond interaction among the H_2O, DMSO and the PVA/PAMAA chains.

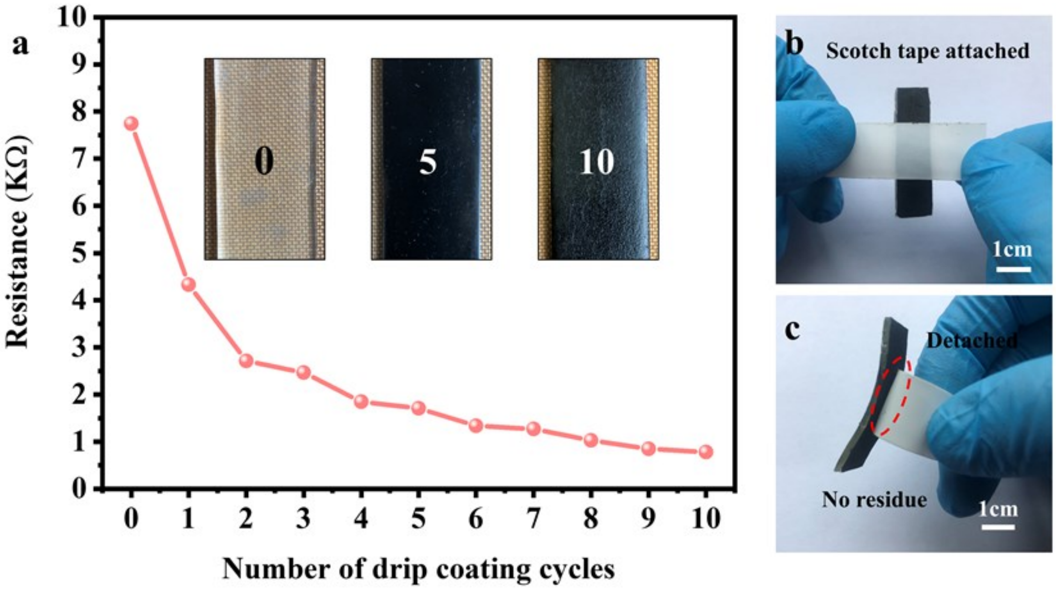

Figure S11. (a) The relationship between the surface resistance of supercapacitor and the number of drop coating cycles. (b) and (c) adhesion strength test. scotch tape attached to the surface of supercapacitor and detached respectively.

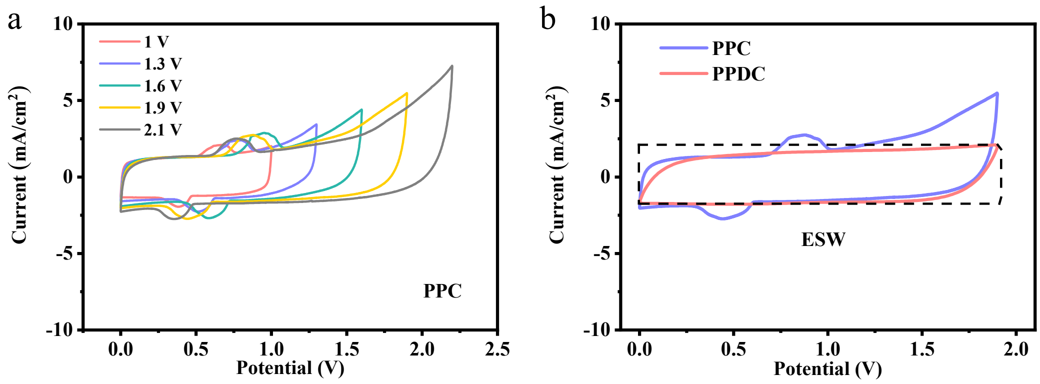

Figure S12. (a) CV curves of the PPChydrogel with different work voltage at 50 mV s^{-1} (b) The Electrochemical stability windows for (ESW) for PPC and PPDC hydrogels.

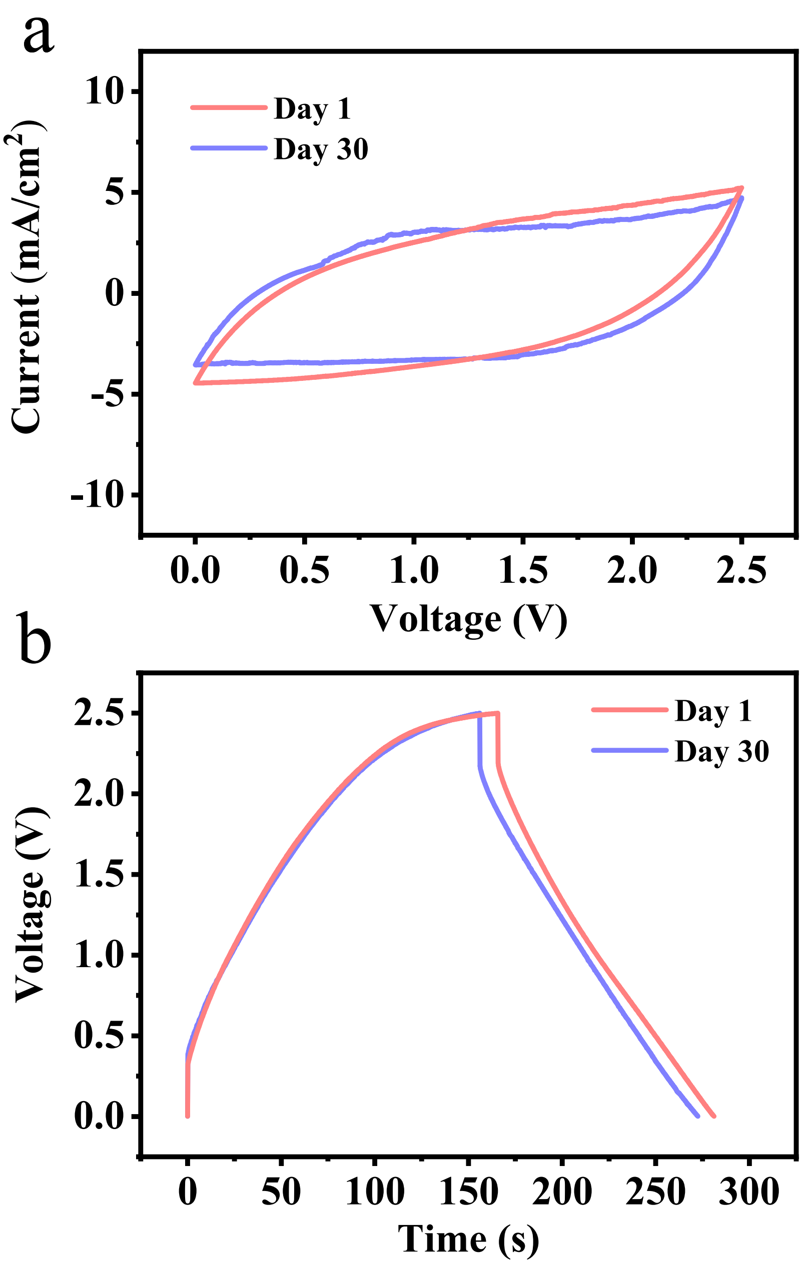

Figure S13. (a) The CV curves and (b) The GCD curves of the supercapacitor compared with storage after 1 day and 30 days.

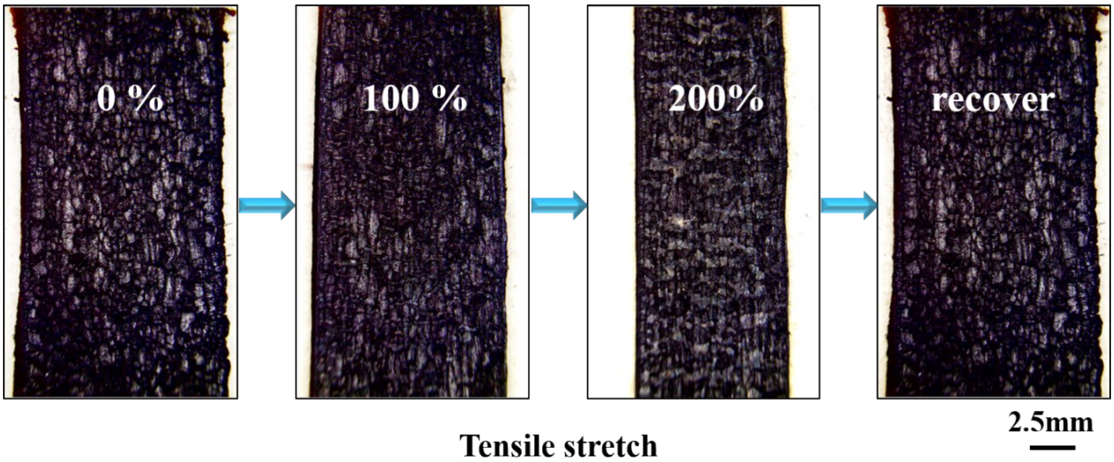

Figure S14. Images of a typical supercapacitor when stretched from 0% to 200% strain, and relaxation after unloading.

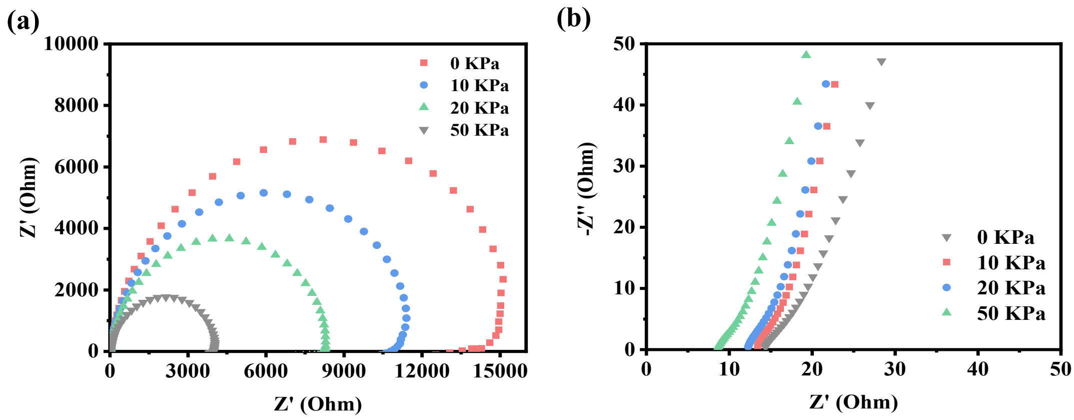

Figure S15. Nyquist impedance plots of the supercapacitor at devise compression

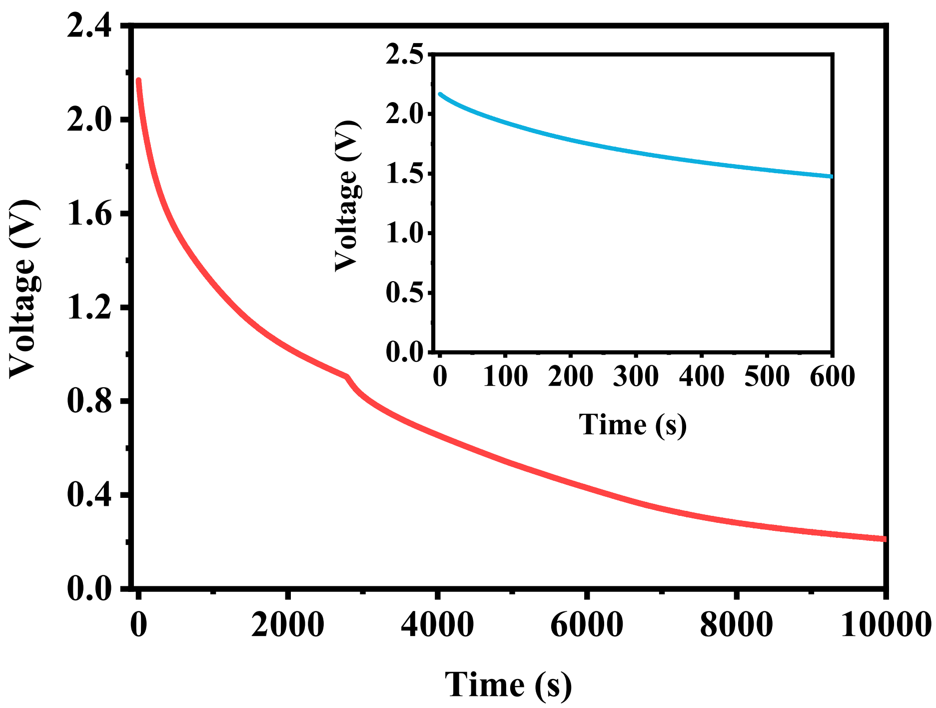

Figure S16. The self-discharge profile of the hydrogel supercapacitor.

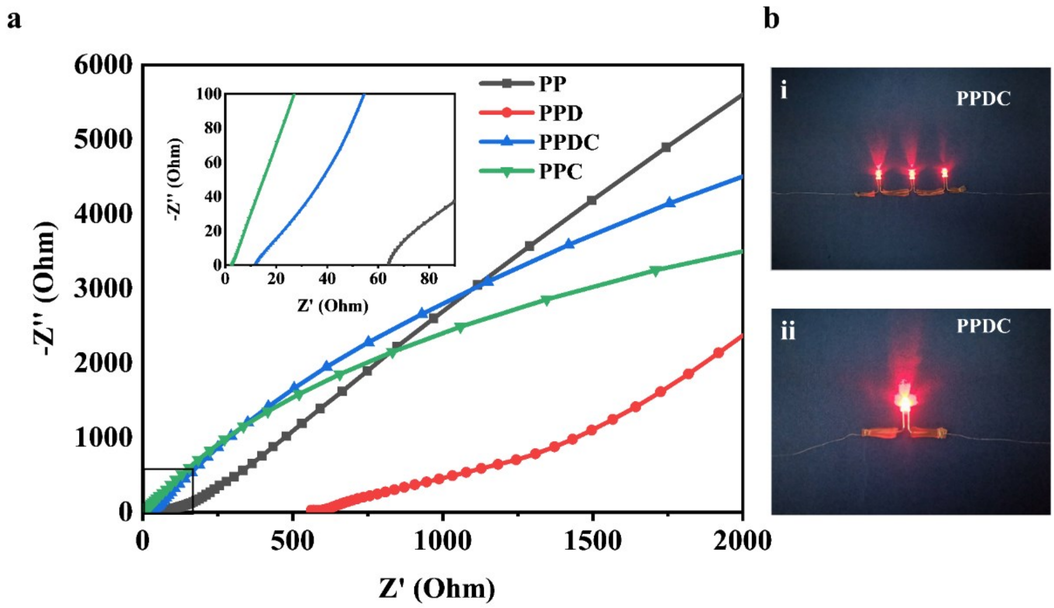

Figure S17. (a)Nyquist impedance plots of the PVA/PAMAA based hydrogel (b) the electrical properties illustration of hydrogel.

The ionic conductivity of the PVA/PAMAA/DMSO/$CaCl_2$ hydrogel was measured by the impedance spectrum using the electrochemical workstation (CHI 660E). The ionic conductivity (σ) was calculated from the equation below:

$$\sigma = \frac{d}{R \cdot A} \tag{1}$$

where A was cross-sectional area of the hydrogel (cm^2); d meant the distance between each two fixed electrodes (cm) and R was the bulk resistance (Ω).

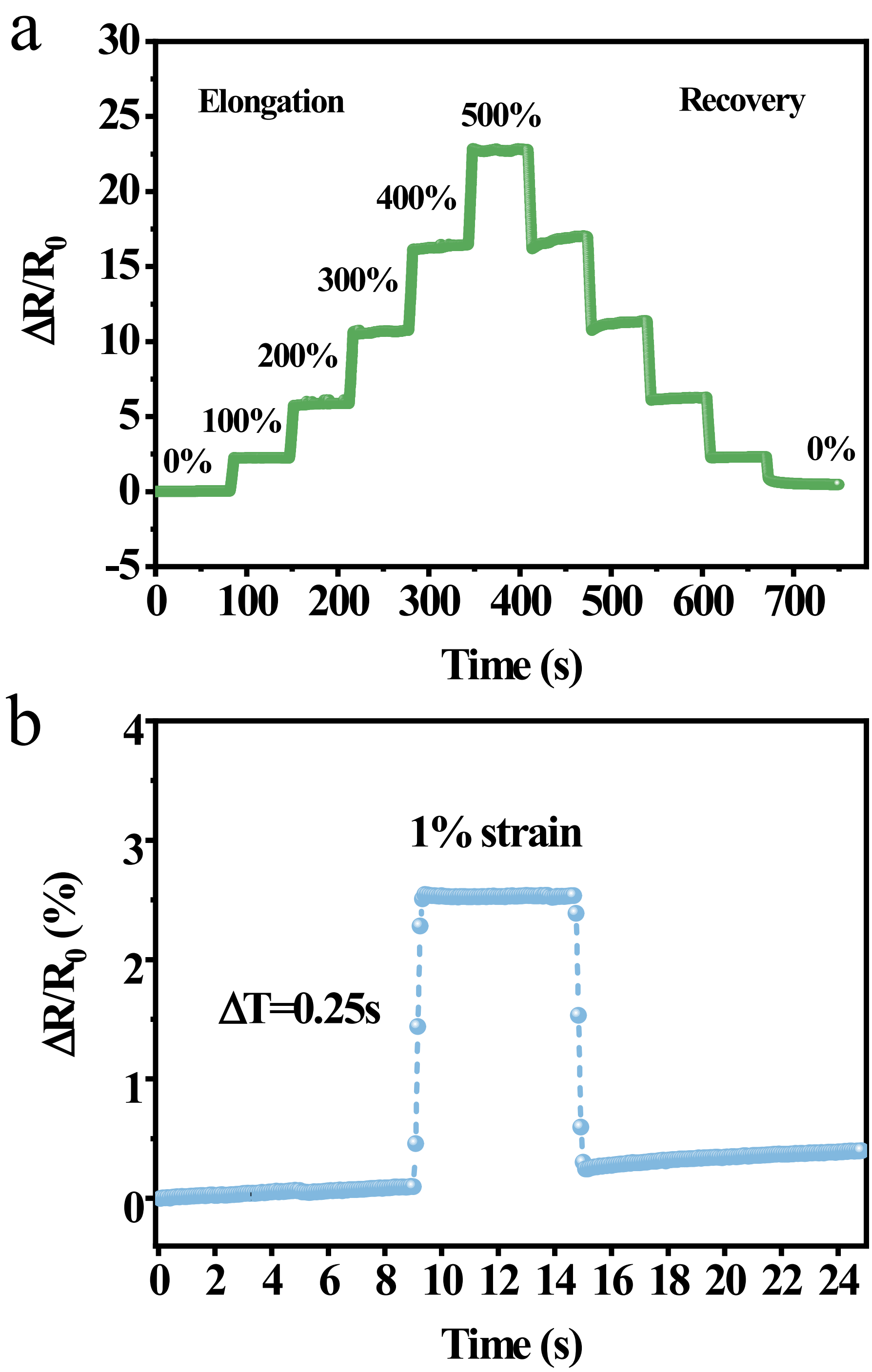

Figure S18. (a) Resistance response of the hydrogel strain sensor stretched to 100%, 200%, 300%, 400% and 500%. (b) The resistance response of the hydrogel strain sensor upon loading and unloading a strain of 1%.

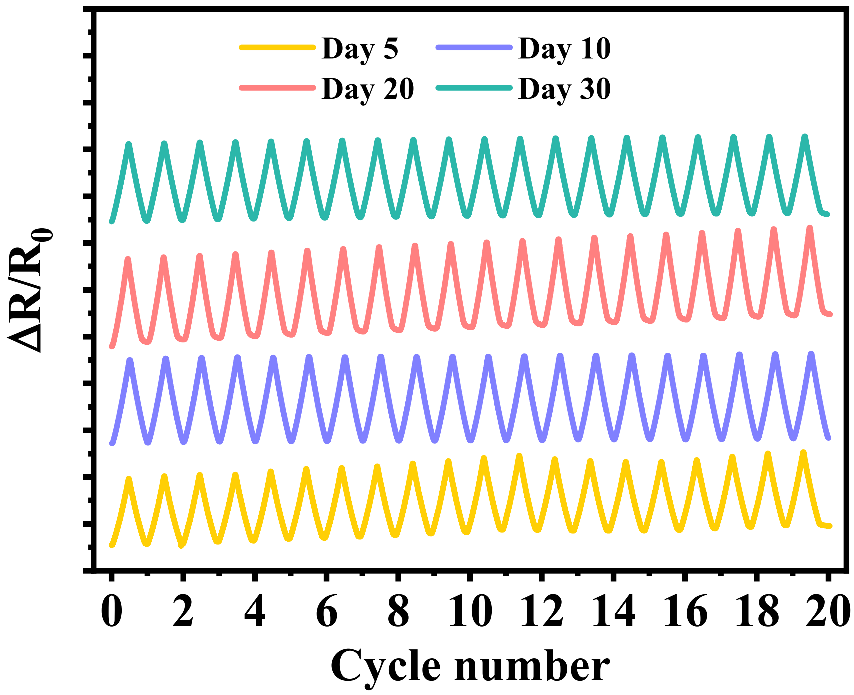

Figure S19. Long-term operation at 50% strain of the PPDC hydrogel sensor over 30 day in ambient condition without specific encapsulation

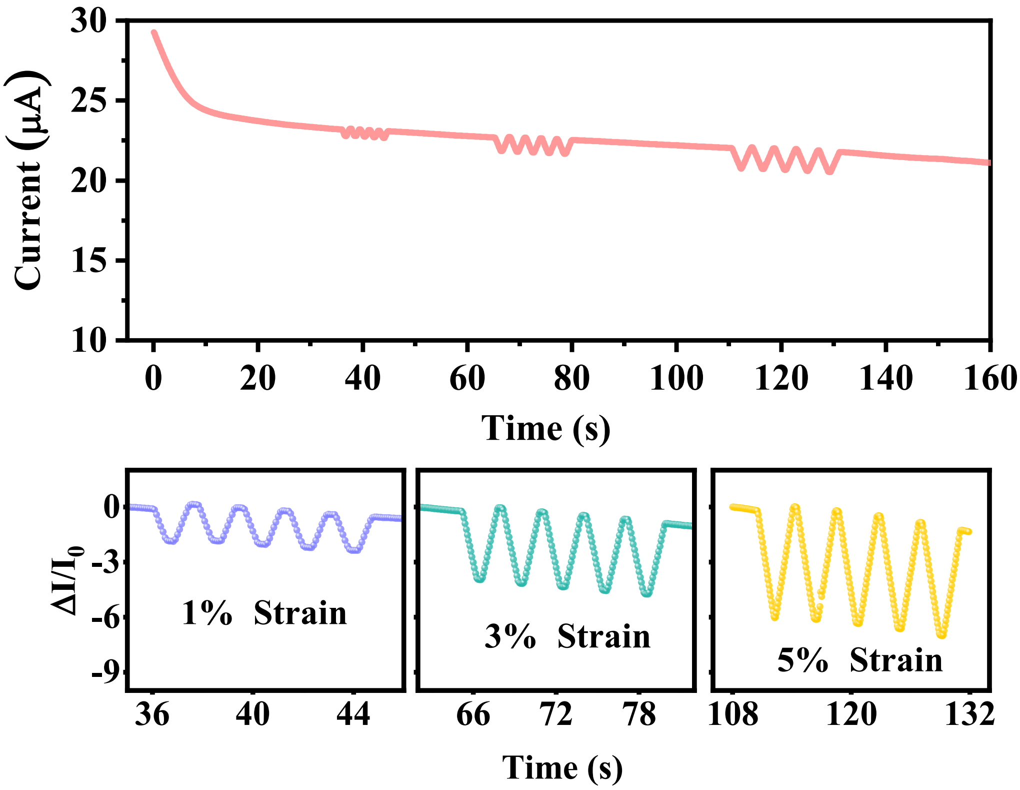

Figure S20. Tiny strain response upon loading and unloading strain of 1%, 3% and 5%.

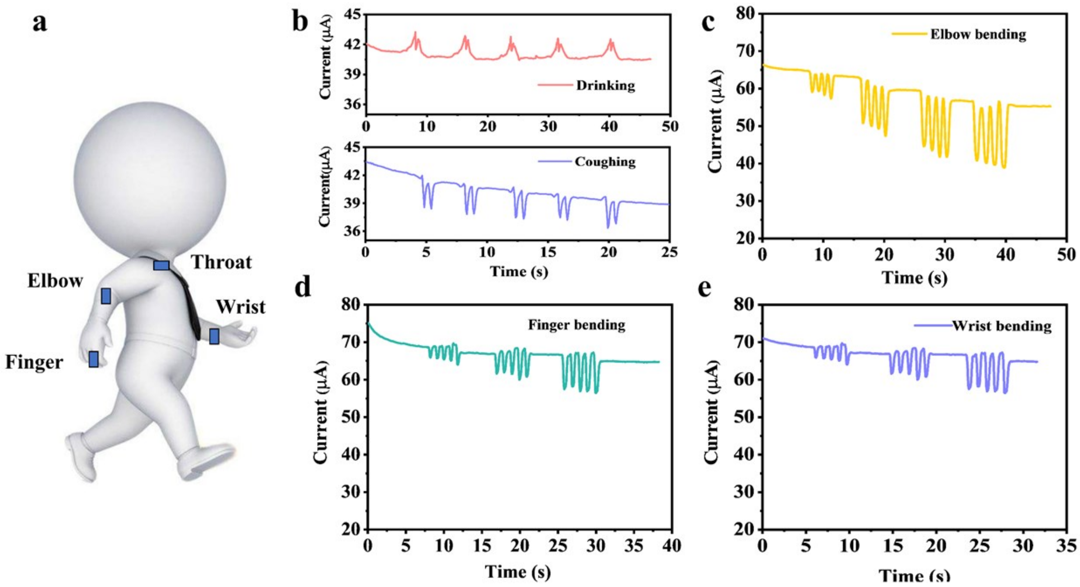

Figure S21. Digital images and corresponding time-current response curves of the self-powered integrated sensing systems in human motion detection. (a) Test schematic, (b) drinking and coughing, (c) elbow bending, (d) finger bending, (e) wrist bending.

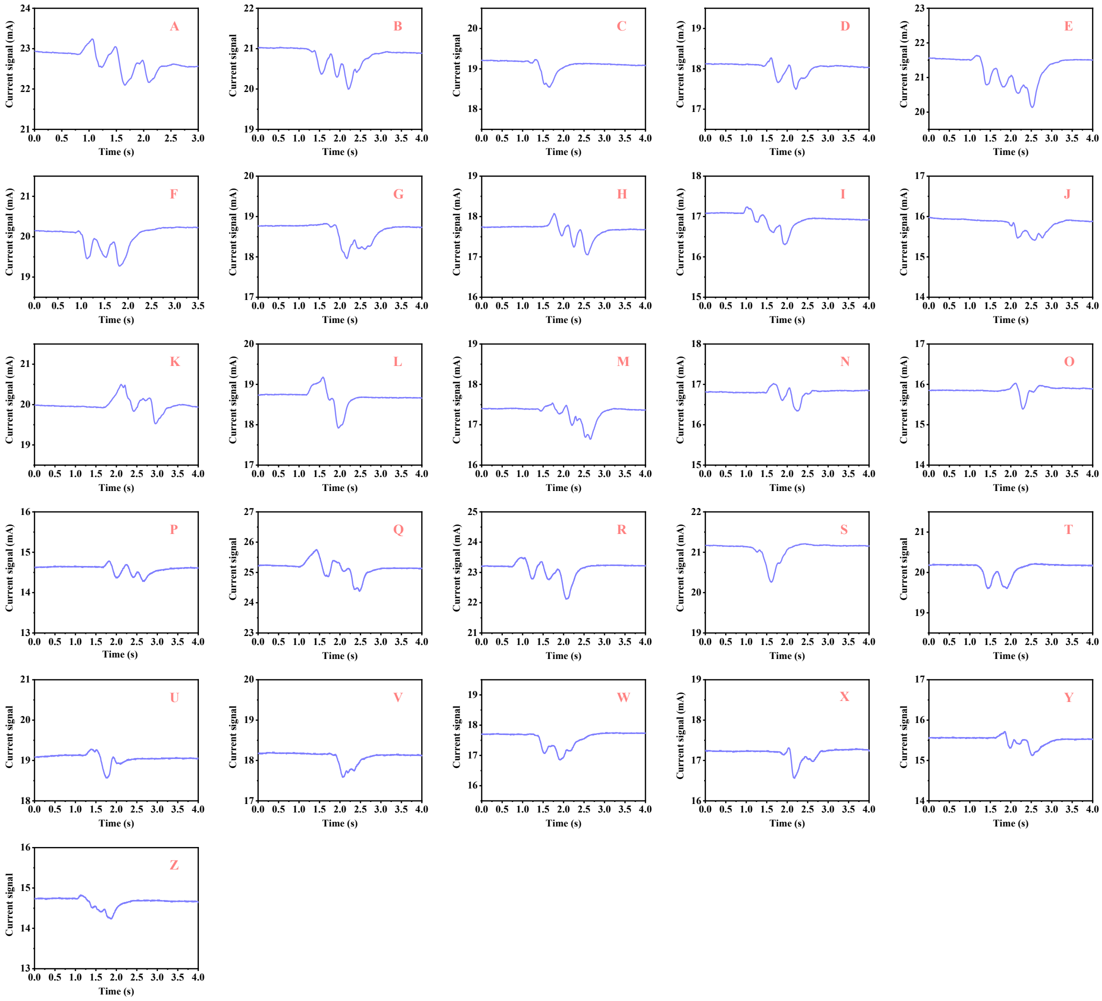
A
B
C
D
E
F
G
H
I
J
K
L
M
N
O
P
Q
R
S
T
U
V
W
X
Y
Z
Current signal (mA)
Current signal
Time (s)

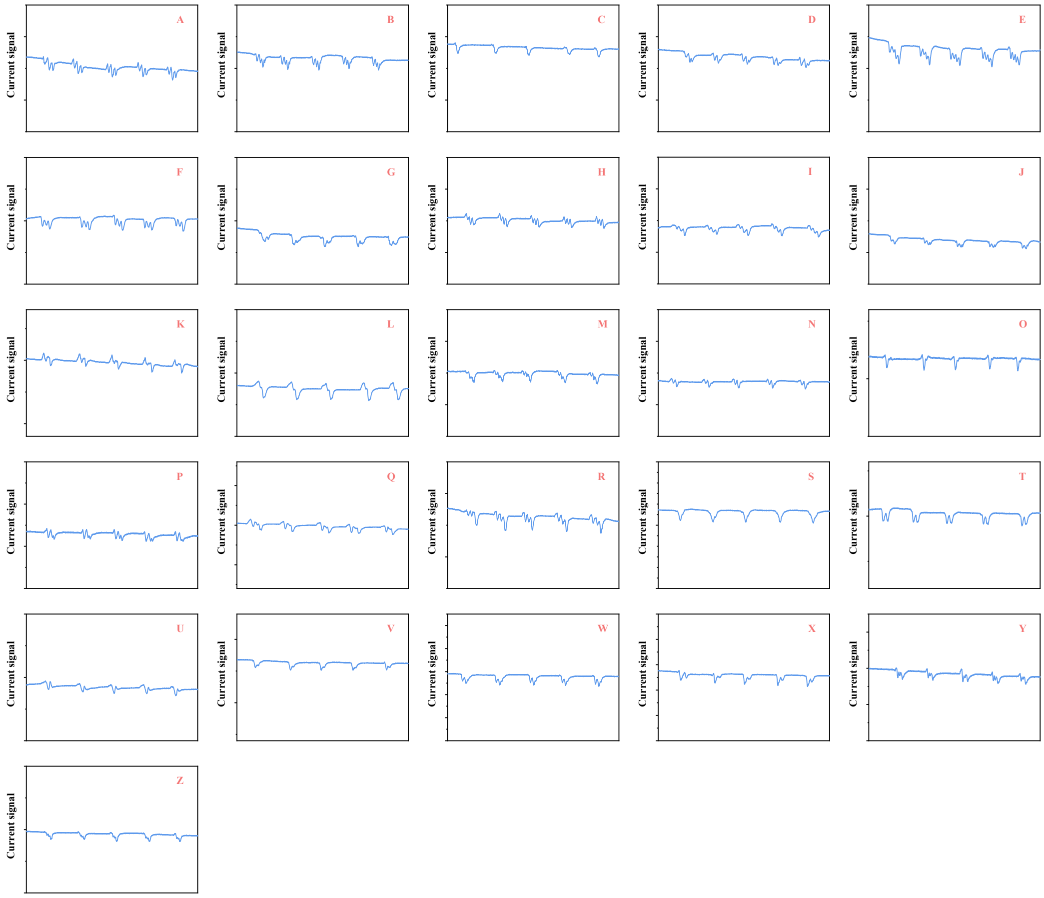

Figure S22. An oscillating electric signals dataset by repeatedly writing 26 different English letter and the PPDC hydrogel sensor was attached to the finger.

For volunteer, repeated each letter 5 times to demonstrate reliability for a total acquisition of 130 sign language hand gesture recognition patterns A total of 130 patterns were randomly selected from the acquired signals to serve as the training set, and the other signals acted as the test set.

Table S1. DFT calculation results of the interaction energy of different system.

Model	Interaction energy (eV)	Interaction energy (kcal/mol)
H_2O/H_2O	-0.311	-7.172
DMSO/H_2O	-0.611	-14.089
PVA-DMSO/H_2O	-1.293	-29.817
PAMAA-DMSO/H_2O	-1.719	-39.640
PVA/PAMAA-H_2O	-1.174	-27.072
PVA/PAMAA-DMSO-H_2O	-2.647	-61.040

Table S2. The experimental ingredients and nomenclatures of PVA/PAMAA/DMSO/$CaCl_2$ hydrogel.

Sample	PVA (g)	AM (g)	AA (g)	Irgacure 2959 (g)	MBA (mg)	Water (g)	DMSO (g)	$CaCl_2$ (g)
PP	0.8	7.9744	0.428	0.2648	5.44	28	0	0
PPC	0.8	7.9744	0.428	0.2648	5.44	28	0	0.70
PPD	0.8	7.9744	0.428	0.2648	5.44	16	12	0
PPDC	0.8	7.9744	0.428	0.2648	5.44	16	12	0.70

Table S3. Ionic conductivity of the PP, PPC, PPD and PPDC hydrogels

Material	Ions conductive (s m^{-1})	Error (s m^{-1})
PP	0.016	0.005
PPD	0.031	0.005
PPC	6.278	0.549
PPDC	2.240	0.143

Table S4. Electrochemical performance of our supercapacitor and other recently reported flexible hydrogel supercapacitors.

Electrode Materials	Electrolyte (Cell Voltage)	Specific capacitance	Energy density	Power density	Cycle retention	Deformation	Ref
MWCNT film	**PVA/PAAM/DMSO/$CaCl_2$ (Gel, 2.5V)**	**93.84 mF cm^{-2}@ 2 mA cm^{-2} 11.73 F cm^{-3} 31.28 F g^{-1}@ 0.67A g^{-1}**	**81.46μWh cm^{-2} 26.07 Wh kg^{-1} 11.73 mWh cm^{-3}**	**2500μW cm^{-2} 800 W Kg^{-1} 312.5mW cm^{-3}**	**75% after 3000 Cycles**	**Stretchable Compressible Bendable**	**This work**
GCP@PPy	CNT-free GCP (Gel, 1V)	885 mF cm^{-2}	123 μWh cm^{-2}	500μW cm^{-2}	93% after 3000 Cycles	Stretchable Bendable	*Adv. Mater.* 2019 [7]
MWCNT film	PVA/PAAM/Gly/NaCl (Gel, 1.5V)	75.75 mF cm^{-2}@ 0.5 mA cm^{-2}	10.52μWh cm^{-2}	0.25 mW cm^{-2}	90.2 after 3000 Cycles	Bendable	*Mater. Horizons* 2020 [8]
MWCNT/MoO_2	ACN-PC-PMMA-$LiClO_4$ (Gel, 1.4V)	33.8 mF/cm^{-2} @0.1mA cm^{-2} 48.3 F g^{-1} @ 0.14A g^{-1} 0.41 F cm^{-3} @1.2mA cm^{-3}	13.16 Wh kg^{-1}	100 W Kg^{-1}	76% after 10000 Cycles	Stretchable Bendable	*ACS Nano* 2020 [9]
PPy/GF	ACN-PC-PMMA-$LiClO_4$ (Gel, 1.4V)	89.6 mF cm-2 @0.6mA cm-2	24 μWh cm^{-2}	2.3 mWcm^{-2}	75% after 1000 Cycles	N/A	*Adv. Funct. Mater* 2018 [10]
C-AL/CNF-5	PVA-H_2SO_4 (Gel, 1.4V)	62.4 F g^{-1} @ 0.5A g^{-1} 231 mF cm^{-2}@ 0.5 mA cm^{-2}	8.6 Wh kg^{-1}	250 W Kg^{-1}	88.5% after 5000cycles	Compressible Bendable	*Adv. Funct. Mater* 2020 [11]
Cu-CAT-NWAs /PPy	PVA-LiCl (Gel, 0.8V)	252.1 mF/cm^{-2} @1.25 mA cm^{-2}	22.4μWh cm^{-2}	1.1 mW cm^{-2}	87% after 5000 Cycles	Bendable	*Adv. Energy Mater.* 2020 [12]
PPy@CNT	Al-alginate/PAAm (Gel, 0.6V)	94.7 mF cm^{-2} @0.1 mA cm^{-2}	0.082 mWh cm^{-3}	5.83mWcm^{-3}	90% after 3000 Cycles	N/A	*Nano Energy* 2019 [13]
PPy film	Agar/HPAAm (Gel, 0.8V)	79.7 mF cm^{-2} @0.2 mA cm^{-2}	N/A	N/A	95.2% after 4000 Cycles	Stretchable	*Angew. Chemie - Int. Ed.* 2019 [14]

PVA-PANI	PVA-H_2SO_4 (Gel, 0.8V)	153 F g^{-1} @ 0.25A g^{-1}	13.6 Wh kg^{-1}	105 W kg^{-1}	90% after 1000 Cycles	Bendable	*Angew. Chemie - Int. Ed.* 2016 [15]
Lignin/PAN	Lignin (Gel, 1V)	129.3 F g^{-1} @ 0.25A g^{-1}	4.49 Wh kg^{-1}	225 W kg^{-1}	N/A	Bendable	*J. Mater. Chem. A* 2019 [16]
CNT-forest	PVA-KCl （Gel，0.8V）	2mF cm^{-2} @ 0.2 mA cm^{-2}	0.1mWh cm^{-3}	100 mW cm^{-3}	92% after 1000 Cycles	Stretchable	*Adv. Energy Mater.*2019 [17]
PAM/SA/CNT/PEDOT	PAM/SA/Na_2SO_4 （Gel，0.9V）	128 mF/cm^{-2}@1mA cm^{-2}	3.6 μWh cm^{-2}	0.2 mW cm^{-2}	75% after 5000 cycle	Stretchable	*Chem. Eng. J. 2020* [18]
Bare CNT	AMPS-co-DMAAm/Laponite/GO （Gel，0.8V）	9 mF cm^{-2}	N/A	N/A	N/A	Stretchable	*Nat. Commun.*2019 [19]
$Ni_{0.25}Mn_{0.75}O$@C	PVA–LiCl （Gel，2.4V）	92.3 mF cm^{-2}@ 2 mA cm^{-2}	4.72 mWh cm^{-3}	61.2 mW cm^{-3}	95.5% after 2000 Cycles	N/A	*Adv. Mater.*,2017 [20]

Table S5. Comparison of our work with other reported flexible hydrogel-based strain sensors

Base gel	Gauge factor (tensile)	Sensing range (%)	Non-volatile	Reference
PVA/PAMAA/DMSO/$CaCl_2$	**6.04**	**1000**	**Yes**	**This work**
PAAm/LiCl	0.84	40	N/A	*Adv. Mater.* 2017 [21]
PVA/SWCNT	1.51	1000	N/A	*Adv. Sci.* 2017 [22]
PANi/ PVA	1.43	100	N/A	*Matter*.2020 [23]
PVA/MXene	25	40	N/A	*Adv. Sci.* 2018 [24]
PAA/Fe_3O_4	3.96	800	N/A	*Small* 2019 [25]
PSS/UPy/PANI	3.4	300	N/A	*Chem. Mater.* 2019 [26]
P(AAm-co-HEMA)/PANI	1.48	300	N/A	*Chem. Mater.* 2018 [27]
PMMA-r-PBA	2.73	850	Yes	*Adv. Energy Mater.*2019 [28]
PAA/PANI/Gly	18.28	269	Yes	*ACS Nano* 2019 [29]
PAAm-TA@CNF-MXene-Gly	8.21	500	Yes	*Adv. Funct. Mater* 2020 [30]
PVA-CNF	1.5	300	Yes	*Adv. Funct. Mater* 2020 [31]

Table S6. Comparison of self-discharge performance of the power supply in present self-power sensory system.

Main material	Opening voltage (V)	Potential attenuation	Power number	Ref
Hydrogel	**2.5V**	**0.691V @600s** **1.7V @6000s**	**1**	**This work**
Hydrogel	1.47 V	0.207 V@800s	2	*Mater. Horizons* 2020 [8]
CNT-PDMS Sponge	N/A	1 V@130s	1	*Nano Energy* 2018 [32]
Graphene Foam	1.4 V	1.2 V@1000s	2	*Adv. Funct. Mater.* 2018 [10]
SPG-PDMS	1 V	1 V@ 480s	1	*Adv. Funct. Mater.*2017 [33]
$NiFe_2O_4$ fiber	1.2 V	1 V@400s	3	*Nanoscale* 2016 [34]
MWCNT/MoO3	1.4	0.8 V @ 15100s	1	*ACS Nano* 2019 [35]

Reference:

(1) Delley, B. From Molecules to Solids with the DMol3 Approach. *J. Chem. Phys.* **2000**, *113* (18), 7756–7764.

(2) Perdew, J. P.; Burke, K.; Ernzerhof, M. Generalized Gradient Approximation Made Simple. *Phys. Rev. Lett.* **1996**, *77* (18), 3865–3868.

(3) Hu, K.; Wu, M.; Hinokuma, S.; Ohto, T.; Wakisaka, M.; Fujita, J. I.; Ito, Y. Boosting Electrochemical Water Splitting: Via Ternary NiMoCo Hybrid Nanowire Arrays. *J. Mater. Chem. A* **2019**, *7* (5), 2156–2164.

(4) Grimme, S.; Antony, J.; Ehrlich, S.; Krieg, H. A Consistent and Accurate Ab Initio Parametrization of Density Functional Dispersion Correction (DFT-D) for the 94 Elements H-Pu. *J. Chem. Phys.* **2010**, *132* (15).

(5) Allouche, A. Software News and Updates Gabedit — A Graphical User Interface for Computational Chemistry Softwares. *J. Comput. Chem.* **2012**, *32*, 174–182.

(6) Nian, Q.; Wang, J.; Liu, S.; Sun, T.; Zheng, S.; Zhang, Y.; Tao, Z.; Chen, J. Aqueous Batteries Operated at −50 °C. *Angew. Chemie* **2019**, *131* (47), 17150–17155.

(7) Chen, C. R.; Qin, H.; Cong, H. P.; Yu, S. H. A Highly Stretchable and Real-Time Healable Supercapacitor. *Adv. Mater.* **2019**, *31* (19), 1–10.

(8) Huang, J.; Peng, S.; Gu, J.; Chen, G.; Gao, J.; Zhang, J.; Hou, L.; Yang, X.; Jiang, X.; Guan, L. Self-Powered Integrated System of a Strain Sensor and Flexible All-Solid-State Supercapacitor by Using a High Performance Ionic Organohydrogel. *Mater. Horizons* **2020**, *7* (8), 2085–2096.

(9) Park, H.; Kim, J. W.; Hong, S. Y.; Lee, G.; Lee, H.; Song, C.; Keum, K.; Jeong, Y. R.; Jin, S. W.; Kim, D. S.; Ha, J. S. Dynamically Stretchable Supercapacitor for Powering an Integrated Biosensor in an All-in-One Textile System. *ACS Nano* **2019**, *13* (9), 10469–10480.

(10) Park, H.; Kim, J. W.; Hong, S. Y.; Lee, G.; Kim, D. S.; Oh, J. hyun; Jin, S. W.; Jeong, Y. R.; Oh, S. Y.; Yun, J. Y.; Ha, J. S. Microporous Polypyrrole-Coated Graphene Foam for High-Performance Multifunctional Sensors and Flexible Supercapacitors. *Adv. Funct. Mater.* **2018**, *28* (33), 1–11.

(11) Chen, Z.; Zhuo, H.; Hu, Y.; Lai, H.; Liu, L.; Zhong, L.; Peng, X. Wood-Derived

Lightweight and Elastic Carbon Aerogel for Pressure Sensing and Energy Storage. *Adv. Funct. Mater.* **2020**, *1910292*, 1–11.

(12) Hou, R.; Miao, M.; Wang, Q.; Yue, T.; Liu, H.; Park, H. S.; Qi, K.; Xia, B. Y. Integrated Conductive Hybrid Architecture of Metal–Organic Framework Nanowire Array on Polypyrrole Membrane for All-Solid-State Flexible Supercapacitors. *Adv. Energy Mater.* **2020**, *10* (1), 1901892.

(13) Liu, Z.; Liang, G.; Zhan, Y.; Li, H.; Wang, Z.; Ma, L.; Wang, Y.; Niu, X.; Zhi, C. A Soft yet Device-Level Dynamically Super-Tough Supercapacitor Enabled by an Energy-Dissipative Dual-Crosslinked Hydrogel Electrolyte. *Nano Energy* **2019**, *58* (December 2018), 732–742.

(14) Wang, Y.; Chen, F.; Liu, Z.; Tang, Z.; Yang, Q.; Zhao, Y.; Du, S.; Chen, Q.; Zhi, C. A Highly Elastic and Reversibly Stretchable All-Polymer Supercapacitor. *Angew. Chemie - Int. Ed.* **2019**, *58* (44), 15707–15711.

(15) Li, W.; Gao, F.; Wang, X.; Zhang, N.; Ma, M. Strong and Robust Polyaniline-Based Supramolecular Hydrogels for Flexible Supercapacitors. *Angew. Chemie - Int. Ed.* **2016**, *55* (32), 9196–9201.

(16) Park, J. H.; Rana, H. H.; Lee, J. Y.; Park, H. S. Renewable Flexible Supercapacitors Based on All-Lignin-Based Hydrogel Electrolytes and Nanofiber Electrodes. *J. Mater. Chem. A* **2019**, *7* (28), 16962–16968.

(17) Cao, C.; Zhou, Y.; Ubnoske, S.; Zang, J.; Cao, Y.; Henry, P.; Parker, C. B.; Glass, J. T. Highly Stretchable Supercapacitors via Crumpled Vertically Aligned Carbon Nanotube Forests. *Adv. Energy Mater.* **2019**, *9* (22), 1–11.

(18) Zeng, J.; Dong, L.; Sha, W.; Wei, L.; Guo, X. Highly Stretchable, Compressible and Arbitrarily Deformable All-Hydrogel Soft Supercapacitors. *Chem. Eng. J.* **2020**, *383* (October), 123098.

(19) Li, H.; Lv, T.; Sun, H.; Qian, G.; Li, N.; Yao, Y.; Chen, T. Ultrastretchable and Superior Healable Supercapacitors Based on a Double Cross-Linked Hydrogel Electrolyte. *Nat. Commun.* **2019**, *10* (1), 1–8.

(20) Zuo, W.; Xie, C.; Xu, P.; Li, Y.; Liu, J. A Novel Phase-Transformation Activation Process toward Ni–Mn–O Nanoprism Arrays for 2.4 V Ultrahigh-Voltage Aqueous

Supercapacitors. *Adv. Mater.* **2017**, *29* (36), 1703463.

(21) Tian, K.; Bae, J.; Bakarich, S. E.; Yang, C.; Gately, R. D.; Spinks, G. M.; in het Panhuis, M.; Suo, Z.; Vlassak, J. J. 3D Printing of Transparent and Conductive Heterogeneous Hydrogel–Elastomer Systems. *Adv. Mater.* **2017**, *29* (10).

(22) Cai, G.; Wang, J.; Qian, K.; Chen, J.; Li, S.; Lee, P. S. Extremely Stretchable Strain Sensors Based on Conductive Self-Healing Dynamic Cross-Links Hydrogels for Human-Motion Detection. *Adv. Sci.* **2017**, *4* (2).

(23) Zhao, Y.; Zhang, B.; Yao, B.; Qiu, Y.; Peng, Z.; Zhang, Y.; Alsaid, Y.; Frenkel, I.; Youssef, K.; Pei, Q.; He, X. Hierarchically Structured Stretchable Conductive Hydrogels for High-Performance Wearable Strain Sensors and Supercapacitors. *Matter* **2020**, *3* (4), 1196–1210.

(24) Zhang, Y. Z.; Lee, K. H.; Anjum, D. H.; Sougrat, R.; Jiang, Q.; Kim, H.; Alshareef, H. N. MXenes Stretch Hydrogel Sensor Performance to New Limits. *Sci. Adv.* **2018**, *4* (6), 1–8.

(25) Zhang, L. M.; He, Y.; Cheng, S.; Sheng, H.; Dai, K.; Zheng, W. J.; Wang, M. X.; Chen, Z. S.; Chen, Y. M.; Suo, Z. Self-Healing, Adhesive, and Highly Stretchable Ionogel as a Strain Sensor for Extremely Large Deformation. *Small* **2019**, *15* (21), 1–8.

(26) Chen, J.; Peng, Q.; Thundat, T.; Zeng, H. Stretchable, Injectable, and Self-Healing Conductive Hydrogel Enabled by Multiple Hydrogen Bonding toward Wearable Electronics. *Chem. Mater.* **2019**, *31* (12), 4553–4563.

(27) Wang, Z.; Chen, J.; Cong, Y.; Zhang, H.; Xu, T.; Nie, L.; Fu, J. Ultrastretchable Strain Sensors and Arrays with High Sensitivity and Linearity Based on Super Tough Conductive Hydrogels. *Chem. Mater.* **2018**, *30* (21), 8062–8069.

(28) Kim, Y. M.; Moon, H. C. Ionoskins: Nonvolatile, Highly Transparent, Ultrastretchable Ionic Sensory Platforms for Wearable Electronics. *Adv. Funct. Mater.* **2019**, *1907290*, 1907290.

(29) Ge, G.; Lu, Y.; Qu, X.; Zhao, W.; Ren, Y.; Wang, W.; Wang, Q.; Huang, W.; Dong, X. Muscle-Inspired Self-Healing Hydrogels for Strain and Temperature Sensor. *ACS Nano* **2019**, acsnano.9b07874.

(30) Wei, Y.; Xiang, L.; Ou, H.; Li, F.; Zhang, Y.; Qian, Y.; Hao, L.; Diao, J.; Zhang, M.; Zhu, P.; Liu, Y.; Kuang, Y.; Chen, G. MXene-Based Conductive Organohydrogels with Long-Term Environmental Stability and Multifunctionality. *Adv. Funct. Mater.* **2020**, 2005135.

(31) Ye, Y.; Zhang, Y.; Chen, Y.; Han, X.; Jiang, F. Cellulose Nanofibrils Enhanced, Strong, Stretchable, Freezing-Tolerant Ionic Conductive Organohydrogel for Multi-Functional Sensors. *Adv. Funct. Mater.* **2020**, *2003430*, 1–12.

(32) Song, Y.; Chen, H.; Chen, X.; Wu, H.; Guo, H.; Cheng, X.; Meng, B.; Zhang, H. All-in-One Piezoresistive-Sensing Patch Integrated with Micro-Supercapacitor. *Nano Energy* **2018**, *53* (August), 189–197.

(33) Li, W.; Xu, X.; Liu, C.; Tekell, M. C.; Ning, J.; Guo, J.; Zhang, J.; Fan, D. Ultralight and Binder-Free All-Solid-State Flexible Supercapacitors for Powering Wearable Strain Sensors. *Adv. Funct. Mater.* **2017**, *27* (39), 1–12.

(34) Li, L.; Lou, Z.; Han, W.; Shen, G. Flexible In-Plane Microsupercapacitors with Electrospun NiFe 2 O 4 Nanofibers for Portable Sensing Applications †. *Nanoscale* **2016**, *8*, 14986.

(35) Park, H.; Kim, J. W.; Hong, S. Y.; Lee, G.; Lee, H.; Song, C.; Keum, K.; Jeong, Y. R.; Jin, S. W.; Kim, D. S.; Ha, J. S. Dynamically Stretchable Supercapacitor for Powering an Integrated Biosensor in an All-in-One Textile System. *ACS Nano* **2019**, *13* (9), 10469–10480.